A Novel Additively 4D Printed Origami-inspired Tunable Multi-layer Frequency Selective Surface for mm-Wave IoT, RFID, WSN, 5G, and Smart City Applications

Yepu Cui, Syed A. Nauroze, Ryan Bahr, Manos M. Tentzeris
ATHENA Lab, Georgia Institute of Technology, USA
{yepu.cui, nauroze, rbahr3}@gatech.edu, etentze@ece.gatech.edu

2021 IEEE/MTT-S International Microwave Symposium - IMS 2021 | 978-1-6654-0307-8/21/$31.00 ©2021 IEEE | DOI: 10.1109/IMS19712.2021.9574806

***Abstract* — This paper presents a novel 4D printed tunable frequency selective surface (FSS) utilizing a multi-layer mirror-stacked "Miura-ori" structure that can be applied in numerous mm-Wave, IoT, RFID, WSN, 5G, and smart city applications. The prototype was fabricated with fully additive hybrid (3D and inkjet) printing processes to realize a flexible two-layer substrate with conductive traces on both top and bottom. The proposed multi-layer/multi-material manufacturing process features very significant strength improvement over paper-based origami structures, while enabling the realization of increasingly complex "morphing" designs that would be otherwise difficult to fabricate using traditional paper-based substrates. The proof-of-concept prototype demonstrates great frequency tunability, angle of incidence (AoI) rejection, and significantly improved insertion loss performance over simpler single-layer Miura-based designs as well as an operability up to much higher mm-wave frequencies up to at least $28\,\mathrm{GHz}$.**

***Keywords* — Origami, 3D printing, inkjet printing, additive manufacturing, frequency selective surface, Miura, flexible, multi-layer.**

I. Introduction

In recent years, frequency selective surfaces (FSSs) have been playing an essential role in emerging technologies such as the internet of things (IoT) [1], [2], RFID [3], wireless sensor network (WSN) [4], 5G [5], [6], smart city [7], etc. To enable effective operability of practical systems in cluttered frequency bands with common time-changing interference, reconfigurable FSSs have to be utilized in order to filter different interfering frequency bands on-the-fly. The common methodology to realize a tunable FSS is to integrate active components such as p-i-n diodes [8], MEMS switches [9], or varactors [10] within the FSS elements. Active components can be responsive and relatively easy to control. However, at the same time, they can be expensive, fragile, and hard to fabricate, limiting the performance and scalability of the reconfigurable FSS.

Another approach to realize tunable FSS is by changing the shape of the substrate mechanically using origami-inspired structures [6], [11], [12], [13]. The origami-based FSS structures can be tuned by folding or unfolding on-demand, effectively changing the equivalent electrical length and the inter coupling of the elements, demonstrating great range of frequency or bandwidth tunability. However, one of the biggest challenges with many origami inspired designs is that they are utilizing paper for the substrate or support material, which is prone to absorbing moisture, tearing, and has significant dielectric losses. Moreover, the fabrication process of paper based origami designs is usually labor intensive and may lack accuracy resulting from the manual cutting and folding processes. For these reasons, it is important to use fully automated processes that utilize durable materials to realize origami-inspired structures to fit the stringent needs of practical mm-wave systems.

This paper demonstrates a mm-wave origami-inspired 4D FSS featuring mirror-stacked "Miura-ori" multi-layer substrate and flexible conductive patterns on both top and bottom. The prototype was fabricated with a fully additive hybrid printing process combining 3D printing and inkjet printing techniques in order to realize a flexible 3D substrate and allow for the deposition of high-resolution dielectric and conductive patterns. The multi-layer design shows a much wider range of frequency tunability, a much better mechanical strength and cycling repeatability, an operability in much higher frequencies up to millimetre-wave as well as a very significant insertion loss improvement over previously reported single-layer designs [6]. The reconfigurability introduced by the origami structure, the better performance achieved by the multi-layer configuration, and the durable prototype realized by the additive fabrication process make this design an ideal easy-to-scale candidate to use in rugged IoT, mm-wave RFID (mmID), WSN, 5G, and smart city applications.

II. Unit cell Design

Previously reported single-layer origami-inspired FSSs under $15\,\mathrm{GHz}$ have shown a very good frequency range tunability and S_{21} performance [11], [12], [13]. However, at higher mm-wave frequencies, the physical size of the FSS structure will be dramatically reduced due to the much shorter wavelength. For example, the size of a $30\,\mathrm{GHz}$ unit cell will be 75% smaller compared to a $15\,\mathrm{GHz}$ unit cell. Previous research on mm-wave single-layer origami FSS has shown a significant performance degradation when measuring the folded sample [6]. This is because the effective area of the folded mm-wave sample with smaller size can not cover the entire beamwidth of the excitation antennas during the measurement, thus leading to leakage that reduces the insertion loss.

To improve the performance of origami-based FSS at mm-wave frequency while maintaining a compact size, a novel mirror-stacked multi-layer Miura-ori FSS element is proposed in Fig. 1 that consists of a single piece 3D printed

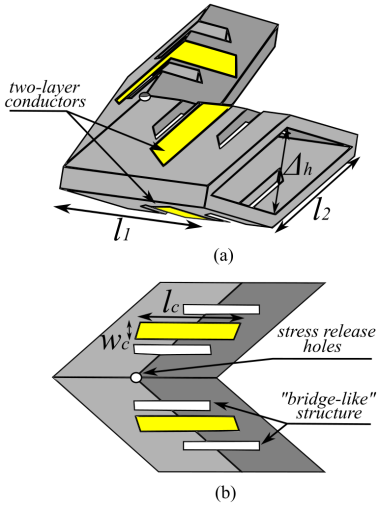

Fig. 1. Mirror stacked multi-layer Miura FSS element: (a) perspective view; (b) top view with stress release design; $l_1 = 5mm$, $l_2 = 7mm$, $w_c = 1mm$, $l_c = 6mm$, substrate thickness $= 0.7mm$.

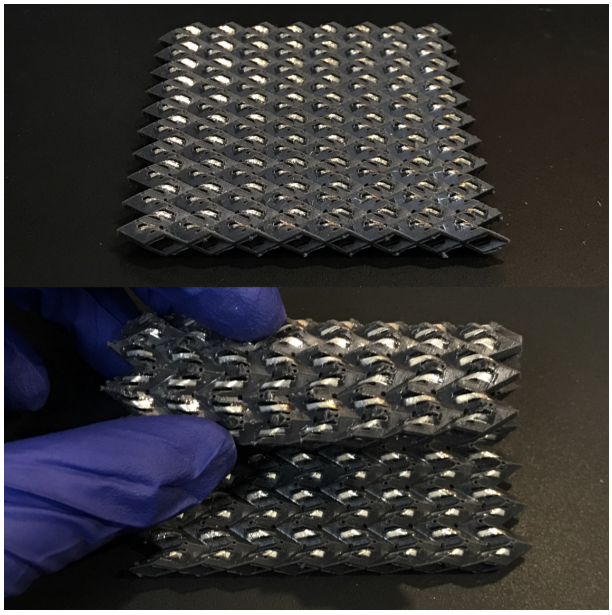

Fig. 2. Fabricated sample of the 8×10 multi-layer Miura FSS.

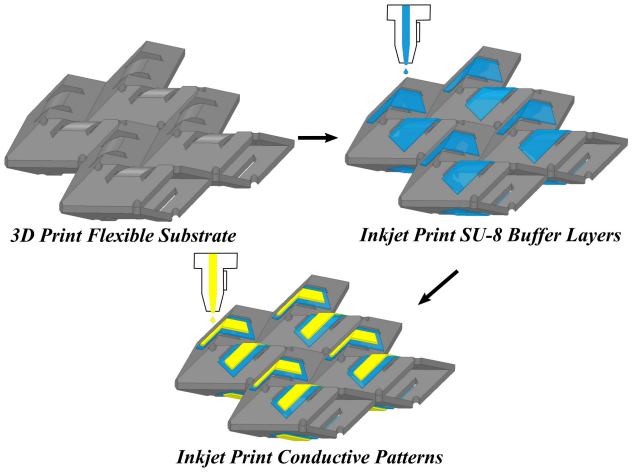

Fig. 3. Schematic of the fabrication process.

substrate with two Miura sheets being stacked, and dipole conductive traces on both top and bottom. The multi-layer configuration doubles the density of the conductive elements, resulting in a larger effective area that improves the insertion loss performance over single-layer designs. The element is designed to take full advantage of 3D printing technology which enables more complicated design elements such as slots, holes, hollows, etc. The stress release slots shown in Fig. 1b form a "bridge-like" structure that reduces the bending stress applied to the conductors when folding the substrate. The stress release holes with $0.4mm$ radius reduce the mechanical stress on the intersection of foldlines.

When compressing the structure from one side, the equivalent length of the conductor will be changed, which in turn causes inductance change that shifts the resonant frequency. The RF performance of the simulated and measured results will be discussed in Section. IV.

III. Fabrication Process

The proof-of-concept 8×10 element multi-layer Miura FSS prototype (Fig. 2) was realized following the steps in Fig. 3 that contains:

- 3D printing of the dielectric substrate.
- Inkjet printing thin SU-8 buffer layers to smooth out the substrate surface and improve conductive layer adhesion.
- Inkjet printing of the conductive layers and sinter with a low temperature gradient.

A. 3D Printed Dielectric Substrate

Previous research [11] has reported that multi-layer origami FSS formed by connecting two piece of papers together can easily break or misalign from the connecting point during folding process. To solve this issue, we printed the substrate in one piece using Formlabs Form2 stereolithography (SLA) 3D printing system. The utilized material was FLGR02 flexible photopolymer that is much more durable than paper-based substrates. The material was characterized using Nicolson-Ross-Weir (NRW) methodology resulting dielectric constant ε_r = 2.78 with loss tangent $\tan\delta$ = 0.03 at 22 GHz. The substrate was printed with 50 µm layer resolution and post processed with standard wash-and-cure process [14] to ensure best consistency and reduce electromagnetic losses. The 8×10 number of elements was limited by the size of the 3D printer's build plate, larger 3D printers are commercially available for larger designs.

B. Inkjet Printed SU-8 Buffer Layers

SLA 3D printing technique built the geometry in a layer-by-layer manner, as a result, the surface was relatively rough (43 µm variation) for inkjet printed conductors (0.8 µm per layer) with periodic "hills" and "valleys" perpendicular to the printing plane. Thus, four layers of inkjet printed

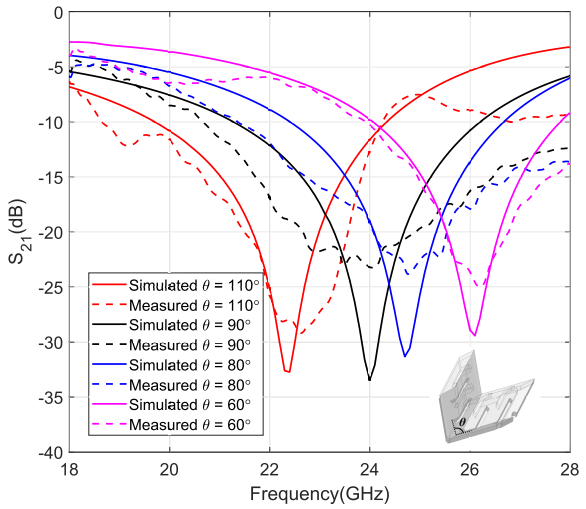

Fig. 4. Simulated and measured frequency response for different folding angles.

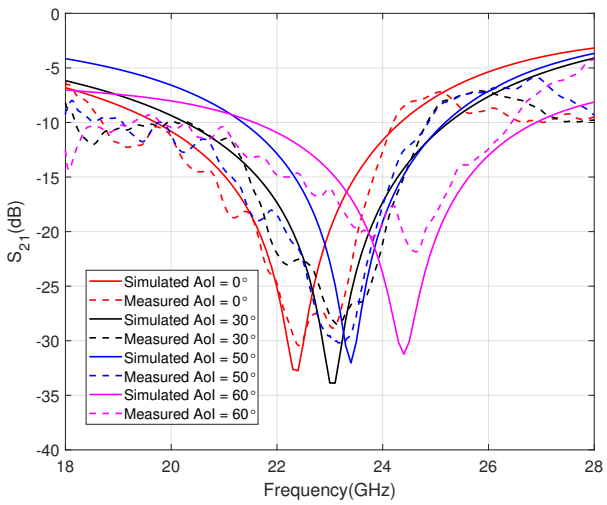

Fig. 5. Simulated and measured frequency response for different incident angles.

MicroChem SU-8 was utilized to reduce the surface roughness variation to $1.6\,\mu m$.

C. Inkjet Printed Conductive Patterns

The conductive pattern was inkjet printed with SunChemical EMD5730 silver nanoparticle (SNP) ink. 90 seconds of UV ozone (O_3) treatment was adopted before printing the conductive SNP traces to improve the wettability and adhesion. Six layers of SNP were utilized for both top and bottom conductor patterns to ensure a good uniformity and conductivity. A low-temperature gradient sintering process was utilized to reduce substrate shrinkage and improve the flexibility of conductor traces.

IV. Simulation and Measurement Results

This mirror-stacked multi-layer Miura-ori FSS prototype was designed and simulated in Ansys HFSS using master and slave boundary conditions with Floquet port excitations. In order to measure the fabricated prototype, two A-INFOMW LB-180400-20-C-KF wideband horn antennas were placed $1.0\,m$ spacing with the FSS sample in the middle, the results were measured on an Anritsu MS46522B VNA set to sweep from $18\,GHz$ to $28\,GHz$.

The simulated and measured frequency response of the mirror-stacked multi-layer FSS for different folding angles θ is shown in Fig. 4. The resonant frequency can be tuned from $22.4\,GHz$ to $26.1\,GHz$ by changing the folding angle θ from $110°$ to $60°$. The frequency shift is caused by the reduced equivalent conductor length during folding, which in turn decreases the equivalent inductance and thus increases the resonant frequency. A performance comparison between multi-layer and single-layer mm-wave Miura FSS is shown in Table 1. The multi-layer configurations shows up to $12\,dB$ better insertion loss performance, especially for lower θ values, and wider frequency tunable range thanks to the improved conductor density.

Table 1. Performance comparison between single-layer and multi-layer mm-wave Miura-based FSS.

	Type	**S_{21} θ=110°**	**S_{21} θ=90°**	**S_{21} θ=80°**	**S_{21} θ=60°**	**Tunable Range**
[6] Single-layer	Miura	-25dB	-22dB	-19dB	-13dB	11.7%
This Work Multi-layer	Miura	-28dB	-23dB	-23dB	-25dB	15.7%

The simulated and measured frequency response of the mirror-stacked multi-layer FSS for different angles of incidence (AoI) is shown in Fig. 5. The prototype shows very good AoI rejection under $50°$. When above $50°$, the resonant frequency will to further shift dramatically due to the significantly changed inter-coupling between top and bottom conductive layers.

V. Conclusion

This paper introduces a state-of-the-art multi-layer mirror-stacked origami-inspired FSS at mm-wave frequencies. A proof-of-concept prototype was fabricated using fully additive hybrid (3D and inkjet) printing process that is automated, fast, accurate, and utilizes durable materials. The multi-layer design doubles the conductor density, dramatically improving the insertion loss performance by up to $12\,dB$ over traditional single-layer designs, with the frequency tunable range being extended as well, making it an ideal easy-to-scale candidate to use in rugged IoT, mm-wave RFID (mmID), WSN, 5G, and smart city applications. The tunability range has the potential to be further improved by adding 3D integrated hinges in future work to simultaneously further enhance the mechanical aspects, such as foldability and repeatability.

Acknowledgment

The authors would like to thank the National Science Foundation (NSF) for their support during this project.

REFERENCES

[1] T. Lin, P. M. Raj, A. Watanabe, V. Sundaram, R. Tummala, and M. M. Tentzeris, "Nanostructured miniaturized artificial magnetic conductors (amc) for high-performance antennas in 5g, iot, and smart skin applications," in *2017 IEEE 17th International Conference on Nanotechnology (IEEE-NANO)*, 2017, pp. 911–915.

[2] H. Jeong, Y. Cui, M. M. Tentzeris, and S. Lim, "Hybrid (3d and inkjet) printed electromagnetic pressure sensor using metamaterial absorber," *Additive Manufacturing*, vol. 35, p. 101405, 2020. [Online]. Available: http://www.sciencedirect.com/science/article/pii/S2214860420307776

[3] F. Costa, M. Borgese, S. Genovesi, L. Buoncristiani, A. Gentile, F. A. Dicandia, A. Monorchio, and G. Manara, "Detection of moving chipless tags by using sar processing," in *2017 IEEE International Conference on RFID Technology Application (RFID-TA)*, 2017, pp. 229–232.

[4] B. Liang, B. Sanz-Izquierdo, J. C. Batchelor, and A. Bogliolo, "Active fss enclosed beam-switching node for wireless sensor networks," in *The 8th European Conference on Antennas and Propagation (EuCAP 2014)*, 2014, pp. 1348–1352.

[5] M. Mantash, A. Kesavan, and T. A. Denidni, "Beam-tilting endfire antenna using a single-layer fss for 5g communication networks," *IEEE Antennas and Wireless Propagation Letters*, vol. 17, no. 1, pp. 29–33, 2018.

[6] Y. Cui, S. A. Nauroze, and M. M. Tentzeris, "Novel 3d-printed reconfigurable origami frequency selective surfaces with flexible inkjet-printed conductor traces," in *2019 IEEE MTT-S International Microwave Symposium (IMS)*, 2019, pp. 1367–1370.

[7] C. Benavente-Peces and I. Herrero-Sebastián, "Worldwide coverage mobile systems for supra-smart cities communications: Featured antennas and design," *Smart Cities*, vol. 3, no. 3, pp. 556–584, Jul. 2020. [Online]. Available: https://doi.org/10.3390/smartcities3030030

[8] M. M. Leingthone and N. Hakem, "Reconfigurable switched-beam antenna using cylindrical bow tie fss window," in *2018 IEEE International Symposium on Antennas and Propagation USNC/URSI National Radio Science Meeting*, 2018, pp. 1851–1852.

[9] Z. Lu, J. She, and X. Yan, "A dual-band reconfigurable fss composite structure based on mems switches," in *2016 11th International Symposium on Antennas, Propagation and EM Theory (ISAPE)*, 2016, pp. 630–632.

[10] A. G. Neto, J. C. e Silva, A. G. Barboza, D. F. Mamedes, I. B. G. Coutinho, and M. de Oliveira Alencar, "Varactor-tunable four arms star bandstop fss with a very simple bias circuit," in *2019 13th European Conference on Antennas and Propagation (EuCAP)*, 2019, pp. 1–5.

[11] S. A. Nauroze, L. S. Novelino, M. M. Tentzeris, and G. H. Paulino, "Continuous-range tunable multilayer frequency-selective surfaces using origami and inkjet printing," *Proceedings of the National Academy of Sciences*, vol. 115, no. 52, pp. 13 210–13 215, 2018. [Online]. Available: https://www.pnas.org/content/115/52/13210

[12] A. Biswas, C. L. Zekios, and S. V. Georgakopoulos, "A dual-band origami fss," in *2019 IEEE International Symposium on Antennas and Propagation and USNC-URSI Radio Science Meeting*, 2019, pp. 2023–2024.

[13] K. Fuchi, J. Tang, B. Crowgey, A. R. Diaz, E. J. Rothwell, and R. O. Ouedraogo, "Origami tunable frequency selective surfaces," *IEEE Antennas and Wireless Propagation Letters*, vol. 11, pp. 473–475, 2012.

[14] (2020) Form wash and form cure automated post-processing. [Online]. Available: https://formlabs.com/wash-cure/